Autoionization of very-high-n strontium Rydberg states

G. Fields,[1] X. Zhang,[1] F. B. Dunning,[1] S. Yoshida,[2] and J. Burgdörfer[2]

[1]*Department of Physics and Astronomy, Rice University, Houston, Texas 77005-1892, USA*
[2]*Institute for Theoretical Physics, Vienna University of Technology, Vienna A-1040, Austria, European Union*

We study, using a combination of experiment and theory, the excitation and decay of very-high-n ($n \sim 280$–430) strontium autoionizing Rydberg states formed by near-resonant driving of the $5s\,^2S_{1/2} \to 5p\,^2P_{1/2}$ core-ion transition. The branching ratio between decay through radiative transitions and through autoionization is explored. Autoionization rates are measured as a function of both the n and ℓ quantum numbers of the Rydberg electron. The nonstationary decay dynamics is studied by creating and manipulating Rydberg wave packets and by varying the laser pulse that drives the core excitation.

I. INTRODUCTION

The original Bohr model of the hydrogen atom treats electrons as point particles moving in classical orbits around the core ion. Whereas this model has now been supplanted by more advanced quantum theories, it still, nonetheless, provides a convenient basis for the discussion of many atomic properties. Furthermore, quantum-classical correspondence suggests that the simple Bohr picture should provide a good description of very highly excited atomic states which have macroscopic dimensions. Indeed, recent advances in the control of very-high-n atomic states using carefully tailored sequences of short electric field pulses have allowed the realization of the classical Bohr atom through the creation of a localized electron wave packet that moves in near-circular orbit about the core ion [1–3]. While for an isolated atom the wave packet eventually spreads out around the orbit, this delocalization can be suppressed by application of a rotating field which results in the creation of a so-called Trojan wave packet whose behavior parallels that of Jupiter's Trojan asteroids [4]. The ability to create localized wave packets whose behavior mimics that of a classical particle suggests that it might be possible to engineer atoms containing two excited electrons each of which moves along a quasiclassical high-n orbit. If these electrons have rather different quantum numbers n_1 and n_2, then due to the very different time scales $\sim n^3$ associated with their motions, the orbit of the "fast" inner electron can become polarized by the presence of the outer electron. As the outer electron moves "slowly" around its orbit, the polarization of the inner electron can change adiabatically so as to follow the motion of the outer electron. The resulting rotating dipole field can then serve to suppress the dispersion of the outer electron wave packet, leading to the formation of a long-lived two-electron excited state [5]. Planetary atoms have been the subject of many experimental and theoretical studies [6–13]. Since planetary atoms are doubly (or multiply) excited states, they can decay not only radiatively but also through autoionization. Autoionization results from energy interchange during collisions between the excited electrons in which one electron acquires energy and is ionized while the second electron loses energy and transitions to a lower state. Therefore, in the semiclassical limit,

$n_1, n_2 \gg 1$, autoionization provides a signature of residual electron-electron scattering. Understanding the autoionization of high-n states is therefore key to developing strategies for the creation of long-lived planetary atoms.

Whereas the simplest two-electron atom is helium, many of the studies of two-electron excited states and of autoionization have focused on the heavier alkaline-earth atoms, i.e., barium, calcium, and strontium [14–21], because radiation at the wavelengths required for their excitation can be more readily generated [22]. Attempts to create planetary atoms have been made in the laboratory by exciting strontium atoms to a high-L Rydberg level ($n \sim 15$ and $L \sim 10$) in the presence of a Stark switching field [23] followed by multiphoton excitation of the inner electron to $6f$ states [7,9,10]. (The rate for autoionization is expected to be suppressed for high-L outer electron states [24,25].) In the limit of high L, the autoionization lifetime should become comparable to, or longer than, the radiative lifetime [26]. For highly excited planetary states, autoionization followed by radiative decay of the inner electron can also become non-negligible [10]. While planetary atoms involving low-lying Rydberg states have rather short lifetimes, the long-term stability in the high-n limit [i.e., in the (semi)classical limit] is still an open question [5,11,13,27].

Interest in the competition between radiative and autoionization decay of highly excited states is, apart from the search for planetary atoms, also motivated by the interest in the reverse process, namely dielectronic recombination (DR) in electron-ion collisions, which is known to be an important recombination mechanism in astrophysical plasmas [28]. Electron-ion collisions can result in the (transient) capture of the incoming electron forming a doubly excited state. The recombined electron can subsequently either autoionize or be stabilized by radiative decay of the excited core electron. Only if the latter channel is operational can DR occur. Laboratory merged-beam measurements of DR [29,30] access primarily low-lying states because the energy spread in the electron beam does not permit individual high-Rydberg states to be resolved. Moreover, electric fields present in the experiment can significantly influence DR due to ℓ mixing [29–31].
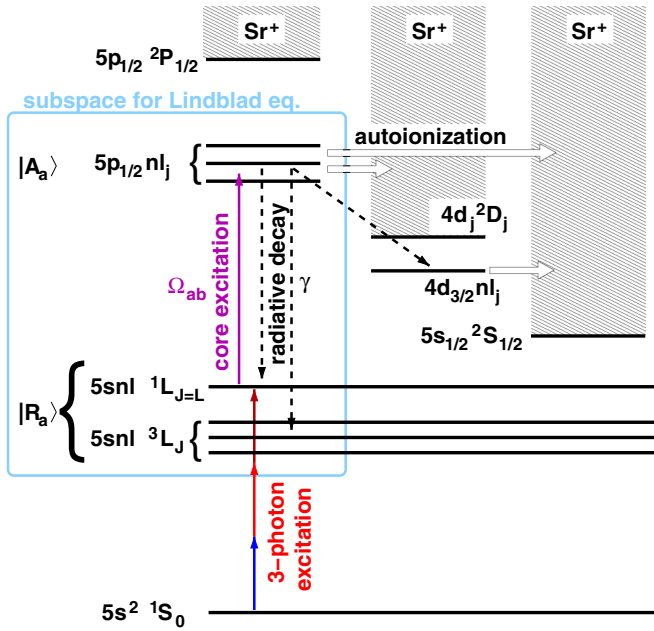
FIG. 1. Energy-level diagram for autoionization and radiative decay of doubly excited Rydberg states of strontium. Initially, the ground-state atom is excited to a singly excited Rydberg state, $5snl\,^1L_J$, in the singlet sector by three-photon excitation (indicated by a sequence of three arrows). The subsequent core excitation of the other valence electron yields doubly excited states, $5p_{1/2}nl_j$ (a single solid arrow). They autoionize (open arrows) or decay radiatively (dashed arrows) to singly excited states, $5sn\ell\,^{2S+1}L_J$, or to doubly excited states, $4d_{3/2}nl_j$. Each shaded area represents the continuum states associated with an ionization threshold corresponding to the indicated energy level of the Sr^+ core ion. The subspace spanning the basis of the master equation [Eq. (6)] is indicated by the light-blue box.

In the present work, we investigate autoionization of very-high-n, $n \sim 280$–450, doubly excited Rydberg states (DERS) using strontium $5snp\,^1P_1$ and $5snf\,^1F_3$ Rydberg atoms, with autoionization induced by excitation of the $5s\,^2S_{1/2} \to 5p\,^2P_{1/2}$ transition in the core ion (Fig. 1). Since the main radiative decay channel of the $5p\,^2P_{1/2}$ core-ion state is to the $5s\,^2S_{1/2}$ ground state (the branching ratio to the $4d\,^2D_{3/2}$ state is about 1/13), the autoionization is principally observed from the $5p_{1/2}np_j$ or the $5p_{1/2}nf_j$ state, with only small contributions from the $4d_{3/2}n\ell_j$ states. For low-n states, autoionization is typically a faster process than radiative decay [32,33]. This results because the outer electron wave function has a relatively large overlap with that of the inner electron. However, since as n increases, this overlap scales as n^{-3}, the autoionization rate should approximately scale as n^{-3}. The current experiments access the high-n limit ($n \gtrsim 300$) where the autoionization rate becomes comparable to or smaller than the radiative decay rate. In this regime, once autoionizing states are excited, they can decay radiatively to a singly excited Rydberg state or autoionize. Therefore, by measuring the surviving fraction of Rydberg states after core excitation, the autoionization rate can be deduced. This regime has been studied previously for highly charged ions for which the radiative decay rate increases with the ion charge Z as Z^4 [34] as well as for doubly excited

states, such as the ^3P state of the oxygen atom which only autoionizes after angular momentum exchange via spin-orbit coupling [35].

In the present experiment, we examine the time evolution of autoionizing Rydberg wave packets created by strong near-resonant core excitation in the presence of strongly excited Rydberg wave packets. The present work also complements earlier studies of DR, but can provide more detailed information with individual n levels being resolved up to $n \sim 450$. Moreover, with careful control of external fields, ℓ dependences in the autoionization and radiative decay rates can be examined. The experimental study is accompanied by theory which employs a Lindblad equation for the reduced density matrix [36] and exterior complex scaling [37].

The paper is organized as follows. In Sec. II, we briefly describe the experiment, followed by the theoretical method in Sec. III. Rydberg autoionization rates in (near) zero electric field are presented in Sec. IV, while the autoionization rates of electric-field-induced wave packets are discussed in Sec. V. Concluding remarks are given in Sec. VI. Atomic units are used throughout unless stated otherwise.

II. EXPERIMENTAL APPROACH

The present apparatus is shown schematically in Fig. 2. Strontium atoms contained in a tightly collimated beam are photoexcited to selected very-high-n, $n \sim 280$–430, $5snp\,^1P_1$ or $5snf\,^1F_3$ states near the center of an interaction region defined by three pairs of copper electrodes. The three-photon excitation scheme that is employed is shown in the inset and utilizes the $5s5p\,^1P_1$ and $5s5d\,^1D_2$ intermediate states [38]. The required radiation at 461, 767, and 893 nm is provided by diode laser systems whose output wavelengths are stabilized using Fabry-Perot transfer cavities locked to a polarization-stabilized HeNe laser. The 461 and 767 nm beams are polarized along the z axis, as indicated in the figure. The 893 nm beam is polarized along the x axis, resulting in the formation of P or F states with $M_J = \pm 1$. The 461 nm beam propagates in the
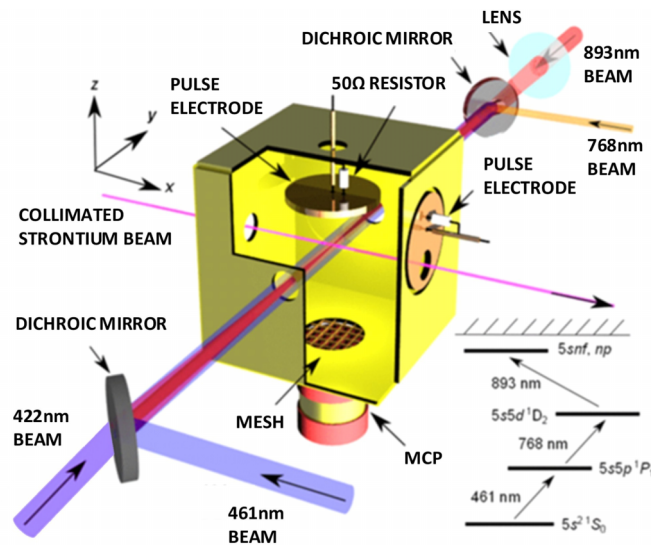

FIG. 2. Schematic diagram of the apparatus. The inset shows the three-photon excitation scheme employed.

reverse direction to the other two beams to minimize Doppler effects associated with atom beam divergence. The strontium atom beam is provided by an oven which can, following collimation, provide a 1-mm-diameter beam with a FWHM divergence of $\sim$4 mrad at densities approaching 10^9 cm^{-3}. Stray fields in the experimental volume are minimized by application of small offset potentials to the electrodes, these being systematically varied to minimize the widths of the nF features which are particularly sensitive to the presence of stray fields. It is estimated that the residual field in the experimental volume is $\lesssim$30 μV cm^{-1}.

Experiments are conducted in a pulsed mode. The output of the 461 nm laser is chopped into a series of pulses of $\sim$100 ns duration and $\sim$10 kHz repetition frequency using an acousto-optic modulator (both other excitation beams remain on at all times). The 461 and 768 nm beams are unfocused and have diameters of $\sim$3 mm. Their intensities, $\sim$10 mW cm^{-2}, were chosen to limit line shifts and broadening associated with effects such as the ac Stark shift and Autler-Townes splitting. The 893 nm beam is focused to a spot with a $1/e^2$ diameter of $\sim$200 μm. Following Rydberg excitation, doubly excited states are generated by a pulse of 422 nm radiation of variable duration tuned to the $5s\,^2S_{1/2} \rightarrow 5p\,^2P_{1/2}$ transition in the core ion. This radiation is provided by a diode laser system whose $1/e^2$ beam diameter at the excitation region is $\sim$1 mm. The laser frequency is stabilized by use of a Fabry-Perot transfer cavity and is referenced to the $5s\,^2S_{1/2}$ ($F' = 2$) $\rightarrow$ $6p\,^2P_{1/2}$ ($F'' = 3$) transition in ^{85}Rb, which lies 440 MHz to the red of the core-ion transition [39], and whose position was determined through saturation-absorption spectroscopy in a heated rubidium cell. One complication in the present work is that as illustrated in Fig. 1, the $5p\,^2P_{1/2}$ core-ion state (with a lifetime of 7.35 ns [40]) can decay not only to the $5s\,^2S_{1/2}$ ground state but also to the long-lived ($\sim$435 ms [39]) $4d\,^2D_{3/2}$ state. The branching ratio for transitions to the $4d$ state is 1 in 13.4, whereupon, if the $5s$-$5p$ transition is saturated, the rate for transitions to the $4d$ state will be $\sim$10^7 s^{-1}. The $4d$ states can also induce autoionization, although the contributions from such autoionization are typically small.

The use of short 461 and 422 nm pulses, and only a small time delay between them, ensures that the great majority of Rydberg atoms remain within the beam of the 422 nm core-excitation laser while it is on. (The mean Rydberg atom velocity, $\sim$4–5 $\times$ 10^4 cm s^{-1}, is such that it typically requires $\sim$1 μs for an atom to travel from the center to the edge of the 422 nm beam.) Following application of the 422 nm laser pulse, and after a time delay of 10 μs to allow any electrons produced through autoionization to be lost to the walls of the interaction region, the number of Rydberg atoms that survive is determined by selective field ionization (SFI), for which purpose a slowly increasing electric field is created in the experimental volume by the application of a linearly increasing positive voltage ramp (rise time $\sim$5 μs) to the lower electrode. Product electrons are accelerated out of the experimental volume and are detected using a microchannel plate. The probability for creation of a Rydberg atom during any experimental cycle is low and data must be accumulated over many such cycles to build up good statistics. While it is challenging to accurately measure the widths of autoionization features that involve small Rydberg atom losses, i.e., features for which effects due to power and

saturation broadening are small, it is not possible using the present apparatus to directly measure the number of ions or electrons produced by autoionization. The fields required to extract ions from the interaction region on reasonable time scales of a few milliseconds are sufficient to field ionize the surviving high-n atoms. The fields necessary to efficiently collect the electrons, which have energies of several electron volts, are even larger. Given that the solid angle ω_c subtended by the microchannel plate at the experimental volume is small, $\omega_c/4\pi \sim 0.01$, in the absence of such fields only a small fraction of the product electrons resulting from autoionization, i.e., those that are initially directed towards the microchannel plate, can be detected, resulting in unacceptably low signal rates.

III. THEORY

The autoionizing resonances of strontium can be analyzed using a two-active electron (TAE) approximation and are governed by the Hamiltonian

$$H = H_1 + H_2 + \frac{1}{|\vec{r}_1 - \vec{r}_2|}. \tag{1}$$

H_i ($i = 1,2$) is the Hamiltonian of the ith electron given by

$$H_i = \frac{p_i^2}{2} + V_{\ell_i}(r_i) + V_{LS}(r_i), \tag{2}$$

where $V_\ell(r)$ is an angular-momentum-dependent model potential representing the Sr^{2+} ion [38]. (We note that since only a few measured energies of ^2P states for the Sr$^+$ ion are available [41], such model potentials are affected by the resulting uncertainty.) The spin-orbit coupling [42] is given by

$$V_{LS}(r) = \frac{1}{2}\alpha^2(\vec{\ell} \cdot \vec{s})\frac{1}{r}V_\ell'(r)\left[1 - \frac{1}{2}\alpha^2 V_\ell(r)\right]^{-2}, \tag{3}$$

with the fine-structure constant α. The last factor serves as a cutoff function to have a well-defined radial wave function for numerical calculations in the limit of $r \rightarrow 0$ [16]. Numerical diagonalization of the Hamiltonian within a finite basis yields a set of eigenstates. Those corresponding to singly excited states are well approximated by the LS coupling scheme $|5snL\,^{2S+1}L_J\rangle$, where L and S are the total angular momentum and spin of the two valence electrons. This is because the electron-electron interaction dominates over the spin-orbit interaction and L and S are (approximately) good quantum numbers. For simplicity, we employ these labels in the following, even though the numerically generated basis contains admixtures from other LS terms. Likewise, autoionizing states are often described by the jj scheme $|n_1\ell_{j_1}n_2\ell_{j_2}\,J\rangle$, where j_1 and j_2 are the total angular momenta of each electron. In particular, for a low-lying inner electron with a highly excited outer electron ($n_1 \ll n_2$), the spin-orbit coupling of the inner electron becomes dominant compared to the electron-electron interaction, and j_1 and j_2 become nearly good quantum numbers. The transformation between the two approximate

basis states (i.e., between the LS- to jj-basis functions) is given by the Wigner-$9j$ symbol,

$$|n_1\ell_{j_1}n_2\ell_{j_2}J\rangle = \sum_{L,S}\sqrt{(2j_1+1)(2j_2+1)(2L+1)(2S+1)}$$

$$\times \begin{Bmatrix} \ell_1 & 1/2 & j_1 \\ \ell_2 & 1/2 & j_2 \\ L & S & J \end{Bmatrix} |n_1\ell_1 n_2\ell_2\,^{2S+1}L_J\rangle.$$

$$(4)$$

The jj-basis states are the eigenstates of the Hamiltonian in the absence of the electron-electron interaction. Since this interaction induces energy and angular momentum exchange between the two electrons, the $n_1\ell_{j_1}n_2\ell_{j_2}$ state can be weakly perturbed and coupled to the continuum $n_1'\ell_{j_1'}'k_2\ell_{j_2'}'$ states. This coupling leads to autoionization.

The energy and the lifetime, i.e., the real and imaginary parts of the complex energies, of doubly excited Rydberg states (DERS) can be calculated using the exterior complex scaling [37]. Accordingly, the eigenvalue equation of the radial wave function is extended in the complex plane by the substitution $r \to re^{i\Theta}$ and, consequently, $p_r \to e^{-i\Theta}p_r$. While the numerical calculations are performed in a box of finite size, the complex scaling with positive rotation angle Θ enforces the outgoing boundary condition on the radial wave function, yielding the extended states with complex energy $E \simeq e^{-i\Theta}k^2/2$ whose imaginary part corresponds to the loss of probability at the boundary. The quasibound autoionizing states have much smaller decay rates (imaginary parts) and appear as isolated resonances that are well separated from the extended states. The complex energies of autoionizing resonances have converged when they are independent of the scaling parameter Θ. The calculated results have been tested for convergence and agree well with the measured lifetimes of low-n autoionizing states $5p_{1/2}ns(J=1)$ [32] and $5p_{1/2}nd(J=3)$ [32] and with the real part of the energy, i.e., the quantum defects, within an error of ~0.01 while slightly overestimating the measured rates of $5p_{1/2}np_j$ states [43]. This method yields, in principle, equivalent results to the multichannel quantum defect theory combined with the R-matrix approach within the framework of a TAE description, commonly used for alkali-earth atoms [16]. This slight difference may be due to the uncertainties in the model potential, as discussed above [Eq. (2)]. Such deviations might be corrected using a model that goes beyond a two-active electron description [44,45]. Figure 3(a) shows a typical energy diagram in the complex plane for strontium ($J=2$) between the $4d_{3/2}$ and the $5p_{3/2}$ states of the Sr$^+$ ion. The black dots extending from the $4d_{j_1}$ ionization limit towards the higher-energy side along a nearly straight line correspond to the continuum states $4d_{j_1}k\ell_{j_2}$ with energy $E \simeq e^{-i\Theta}k^2/2$ (Θ is set to 0.01π). The series of autoionizing states with configurations $5p_{j_1}np_{j_2}$ and $5p_{j_1}nf_{j_2}$ are clearly recognizable as they are well isolated from the continuum states with the same energy. The autoionization rates Γ can be estimated from the imaginary part of the complex energies, $\Gamma = 2\text{Im}(E)$, and follow the approximate scaling of n_{eff}^{-3} [Fig. 3(b)]. This is consistent with the fact that in the semiclassical limit ($n \gg 1$), the electron-electron interaction is approximately proportional to the overlap between the
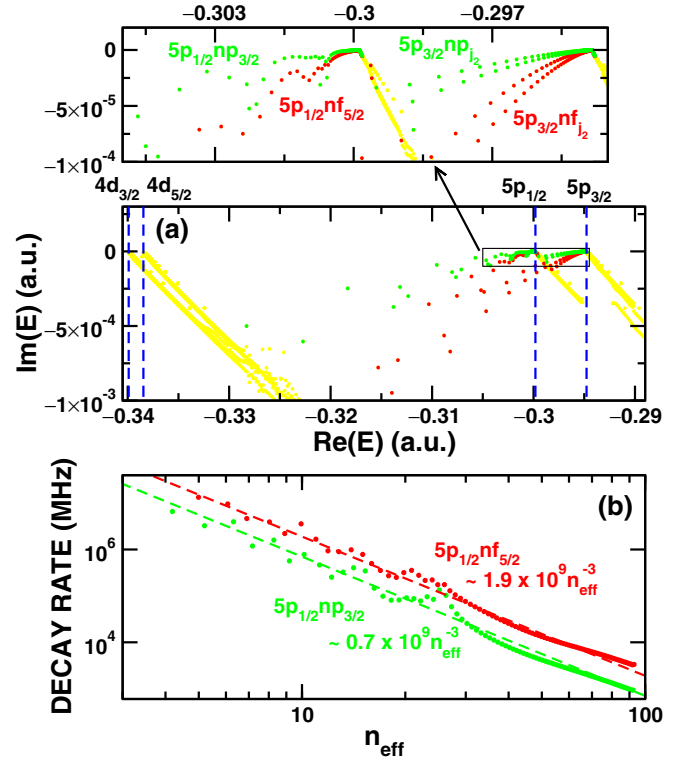

FIG. 3. (a) Calculated complex eigenenergies between the $4d\,^2D$ and the $5p\,^2P$ ionization thresholds. Yellow (light gray) dots: extended continuum states; green (gray) dots: $5p_{j_1}np_{j_2}$ autoionizing resonances; red (black) dots: $5p_{j_1}nf_{j_2}$ autoionizing resonances. The top frame shows a blow-up of the region near the $5p\,^2P$ threshold. (b) Autoionization lifetimes of the $5p_{1/2}n\ell_j$ eigenstates as a function of effective quantum number n_{eff}.

core and Rydberg electron wave functions, which scales as n_{eff}^{-3}. The fluctuations about this power-law scaling seen for $n < 90$ [Fig. 3(b)] are due to perturbers and mixing between channels. Since in the calculations no perturbers, such as $5p_{3/2}n\ell_j$ states, are found in the neighborhood of high-n (>270) states [Fig. 3(a)], this n scaling is used to extrapolate the autoionization rates to higher n. The quantum defects of the autoionizing states can be calculated by fitting the real part of the complex energy to the Rydberg-Ritz formula with [46]

$$n_{\text{eff}} = n - \delta - \frac{\beta}{2(n-\delta)^2}.$$

$$(5)$$

For the $5p_{1/2}np_j$ and $5p_{1/2}nf_j$ states, the autoionization rates and the fitting parameters of the Rydberg-Ritz formula are listed in Table I. The calculations show that the $5p_{1/2}nf_j$ states have larger autoionization rates than the $5p_{1/2}np_j$ states [Fig. 3(b)]. This is because, for small ℓ, the phase shift of the radial wave function given by the quantum defect sensitively influences the radial electron-electron interaction integral for low ℓ. Only for larger ℓ does the semiclassical estimate $\Gamma \propto \ell^{-5}$ [24], which follows from the radially decreasing overlap of (hydrogenic) wave functions, apply.

For strontium, the radiative lifetime of the $5p\,^2P_{1/2}$ core-ion state is about 7.35 ns. Consequently, around $n_{\text{eff}} \simeq 350$, the radiative decay rate becomes comparable to the autoionization rate. For high n, therefore, a significant fraction of autoionizing

TABLE I. Autoionization rates and the fitting parameters for the Rydberg-Ritz formula [Eq. (5)] for the autoionizing states $5p_{1/2}np_j$ and $5p_{1/2}nf_j$. For the quantum defect δ, only the fractional part, $\bar{\delta} = \delta - \lfloor \delta \rfloor$, is listed.

	Γ (MHz)	δ	β
$5p_{1/2}np_{1/2}(J = 0)$	$1.1 \times 10^9 n_{\text{eff}}^{-3}$	0.669	−2300
$5p_{1/2}np_{1/2}(J = 1)$	$0.55 \times 10^9 n_{\text{eff}}^{-3}$	0.927	−50
$5p_{1/2}np_{3/2}(J = 1)$	$0.55 \times 10^9 n_{\text{eff}}^{-3}$	0.806	−38
$5p_{1/2}np_{3/2}(J = 2)$	$0.7 \times 10^9 n_{\text{eff}}^{-3}$	0.836	−138
$5p_{1/2}nf_{5/2}(J = 2)$	$1.9 \times 10^9 n_{\text{eff}}^{-3}$	0.193	−271
$5p_{1/2}nf_{5/2}(J = 3)$	$0.8 \times 10^9 n_{\text{eff}}^{-3}$	0.145	−68
$5p_{1/2}nf_{7/2}(J = 3)$	$1.7 \times 10^9 n_{\text{eff}}^{-3}$	0.272	−299
$5p_{1/2}nf_{7/2}(J = 4)$	$1.3 \times 10^9 n_{\text{eff}}^{-3}$	0.134	−165

states radiatively decays to a singly excited Rydberg state of Sr instead of to Sr$^+$. In order to evaluate the spectra for the surviving Rydberg population, both decay processes have to be taken into account. We theoretically simulate the excitation and decay dynamics of the autoionizing Rydberg states by solving the master equation for the reduced density operator ρ of the quasi-two-electron system in the Lindblad form [36],

$$\frac{d}{dt}\rho = -i(H_{\text{eff}}\rho - \rho H_{\text{eff}}^{\dagger})$$
$$+ \sum_a \left(K_a \rho K_a^{\dagger} - \frac{1}{2}\rho K_a^{\dagger}K_a - \frac{1}{2}K_a^{\dagger}K_a\rho \right). \quad (6)$$

The Hamiltonian for the subspace containing singly excited Rydberg states $|R_a\rangle = |5sn\ell\,^{2S+1}L_J\rangle$ and the DERS $|A_a\rangle = |5p_{1/2}n\ell_j\,J\rangle$ (Fig. 1) is defined as

$$H_{\text{eff}} = \sum_a E_a|R_a\rangle\langle R_a| + \sum_a \mathcal{E}_a|A_a\rangle\langle A_a|$$
$$+ \frac{1}{2}\sum_{a,b}\Omega_{ab}(|A_a\rangle\langle R_b| + |R_b\rangle\langle A_a|), \quad (7)$$

with Rabi frequencies Ω_{ab} for the laser-driven core excitation. Equation (6) describes a twofold open quantum system (see Fig. 1): it is open to spontaneous photoemission described by the Lindblad operators

$$K_a = \sum_b \sqrt{\gamma_{ab}}|R_b\rangle\langle A_a|, \quad (8)$$

with γ_{ab} the spontaneous-emission rate preserving the overall probability, Tr(ρ), but dissipating energy and inducing decoherence, and it is also open to outgoing probability flux by autoionization described by the non-Hermitian H_{eff} with complex energies $\mathcal{E}_a$. The three-photon excitation of a singly excited Rydberg state from the ground state is not explicitly included (i.e., the initial state is assumed to be already excited to a Rydberg state). The unperturbed energies $\mathcal{E}_a$ of the autoionizing states are evaluated by complex scaling (Table I). Correspondingly, the Hamiltonian is non-Hermitian and the loss of probability in the resulting nonunitary evolution represents the decay of autoionizing states to a continuum electron plus a Sr$^+$ ion (open arrows in Fig. 1). The radiative decay processes (dashed arrows in the figure) are accounted for by the Lindblad superoperators associated with K_a [Eq. (8)].

In the experiment, the laser polarizations are configured to excite the initial Rydberg states with $|M_J| = 1$. While the dipole selection rules associated with the core excitation are $\Delta J = 0, \pm 1$ and $\Delta M_J = 0$, radiative decay populates other M_J levels. All these accessible states need to be included in the basis of the master equation [Eq. (6)]. Specifically, for the core excitation of the $5snp\,^1P_1$ state, the basis states are chosen to be $5snp\,^1P_1$ and $5snp\,^3P_J$ ($J = 0,1,2$) for the Rydberg states and $5p_{1/2}np_{1/2}$ ($J = 0,1$) and $5p_{1/2}np_{3/2}$ ($J = 1,2$) for the autoionizing states including all M_J levels. For the core excitation of the $5snp\,^1F_3$ state, the basis states are chosen to be $5snf\,^1F_3$ and $5snf\,^3F_J$ ($J = 2,3,4$) for the Rydberg states and $5p_{1/2}np_{5/2}$ ($J = 2,3$) and $5p_{1/2}np_{7/2}$ ($J = 3,4$) for the autoionizing states. Since in the experiment the core excitation pulse is short ($\sim$100 ns), i.e., at most two Rabi cycles for the laser intensities used in this study, the states with small $|M_J|$ are expected to dominantly contribute to the dynamics. Therefore, for the F state, the states with $|M_J| \leqslant 2$ are included in the simulations. For simplicity, the temporal shape of the laser pulse is assumed in the simulations to be rectangular, i.e., the Rabi frequencies are assumed to be constant. The simulations are continued after termination of the 422 nm core-excitation pulse to follow the subsequent decay of the doubly excited Rydberg states though radiative decay and autoionization.

IV. ZERO-FIELD AUTOIONIZATION RATES

Figures 4(a) and 4(b) display representative Rydberg atom loss spectra for neighboring $5s384f\,^1F_3$ and $5s387p\,^1P_1$ singly excited Rydberg states after exposure, for 100 ns, to the (core-exciting) 422 nm laser as it is scanned across the core-ion transition. Sizable loss features are evident in both spectra. [While the peak losses are $\sim$40% in the present examples (Fig. 4), the 422 nm laser intensities used in the bulk of the measurements reported here were selected such that the maximum Rydberg losses on resonance amounted to $\lesssim$25% to limit distortion of the spectra due to saturation effects.] The width of the $5s384f\,^1F_3$ autoionizing feature is larger than that of the neighboring $5s387p\,^1P_1$ feature. The calculated spectra are also shown in Figs. 4(a) and 4(b) and agree well. The calculated surviving Rydberg population includes all Rydberg states in the singlet and triplet sectors, while the population in the autoionizing levels is removed. To visualize the positions of autoionizing resonances, the occupation probabilities in the different autoionizing levels immediately after the conclusion of the 422 nm excitation pulse are shown in Figs. 4(c) and 4(d). For $n = 387$, the autoionization rates of the $5p_{1/2}np_j$ states are $\sim$10-12 MHz and those of the $5p_{1/2}nf_j$ states for $n = 384$ are $\sim$20-30 MHz. The widths of the autoionizing lines are broadened by radiative decay, $\gamma/(2\pi) \simeq 22$ MHz, and by power broadening (Rabi frequencies $\sim$4-8 MHz). Each individual resonance is peaked at a different position, indicating varying strengths of electron-electron interaction, but their detuning from the isolated core transition appears to be, at most, $\sim$23 MHz [Figs. 4(c) and 4(d)]. The line shape of each resonance is in general not Lorentzian. For example, the $5p_{1/2}np_{1/2}(J = 1)$ state is slightly broadened to the blue. This results because after a fraction of the $5p_{1/2}np_{3/2}(J = 2)$ states are deexcited to triplet $5s387p\,^3P_J$ states, the $5p_{1/2}np_{1/2}(J = 1)$ state can be resonantly excited from the triplet states with
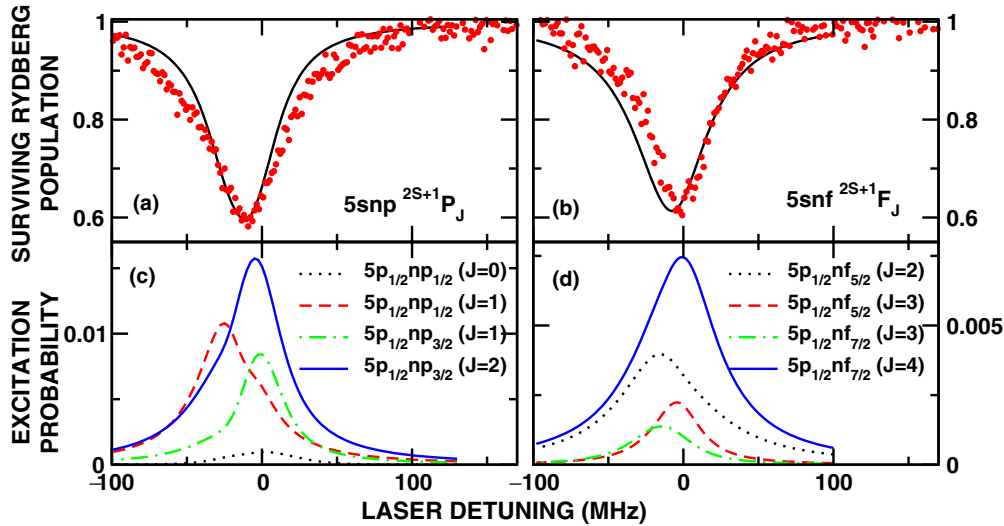
FIG. 4. Measured (dots) and calculated (line) Rydberg atom loss spectra for (a) the 387 $^1P_1$ and (b) 384 $^1F_3$ states as the 422 nm autoionizing laser is scanned across the $5s\,^2S_{1/2} \rightarrow 5p\,^2P_{1/2}$ core-ion transition. The duration of the 422 nm laser pulse is 140 ns. The calculated excitation spectra at the end of the core-excitation pulse starting from (c) the $5s5p\,^1P_1$ state and (d) the $5s5f\,^1F_3$ state. While the excitation spectra [(c),(d)] are time dependent, the surviving Rydberg populations [(a),(b)] are evaluated in the stationary limit after all doubly excited states have decayed radiatively or via autoionization.

nearly zero detuning [the quantum defects of the triplet states are $\sim$2.88 and are very similar to that of the $5p_{1/2}np_{1/2}(J=1)$ state, 2.93]. Such asymmetric line shapes are typically seen for high laser intensities for which the population in the repumped autoionizing states becomes non-negligible.

Figure 5 shows the width of the decaying doubly excited Rydberg state measured through the surviving Rydberg population in the $5snp\,^1P_1$ and $5snf\,^1F_3$ states as a function of n_{eff}^{-3} for values of n in the range 285 to 430. To obtain these data, the
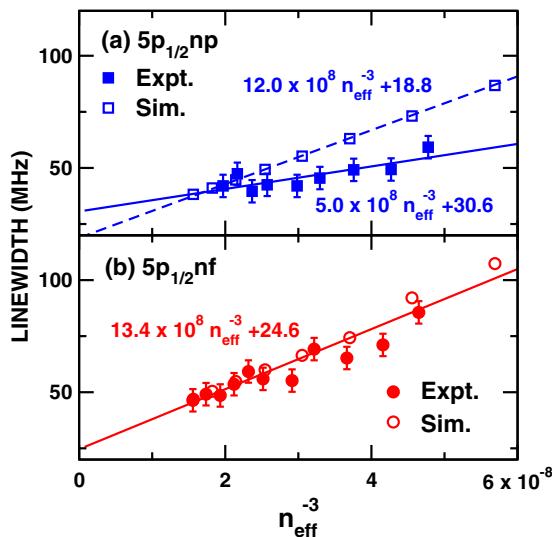

FIG. 5. Measured (filled symbols) and calculated (open symbols) widths of (a) $5p_{1/2}np_j$ and (b) $5p_{1/2}nf_j$ autoionization features as a function of $1/n_{\mathrm{eff}}^3$. For $5snp\,^1P$, the data are fitted separately for the measured (solid line) and the simulated (dashed line) results, while a single linear fit is performed for $5snf\,^1F$. The extrapolation $n_{\mathrm{eff}}^{-3} \rightarrow 0$ provides an estimate for the radiative decay rate of the isolated core ion.

linewidths for the various states were measured as a function of the power of the (core-exciting) 422 nm laser (not shown) and were extrapolated to zero power using the approach described earlier by Gallagher and co-workers [47], which accounts for the nonlinear growth of broadening as a function of transition strength due to depletion broadening. However, since data were only recorded for small autoionization losses, such corrections to the measured linewidths were small, typically $\lesssim$10-20 %. The extrapolated values are shown in Fig. 5 and scale linearly with n_{eff}^{-3}. The calculations show the same linear dependence on n_{eff}^{-3} and, while theory somewhat overestimates the measured linewidth for the $5snp\,^1P_1$ state, agreement for the $5snf\,^1F_3$ state is good. When extrapolated to the limit of $n_{\mathrm{eff}} \rightarrow \infty$, the measured widths converge to $\sim$24 MHz for the $5snf\,^1F_3$ state, which is somewhat larger than the width of the $5s$-$5p$ radiative transition in an isolated core ion, $\sim$21.7 MHz [40]. For the $5snp\,^1P_1$ state, the measured linewidth converges to $\sim$30 MHz, while the calculation yields $\sim$19 MHz. This discrepancy may result partly from the overestimated autoionization rate as mentioned earlier and partly because the surviving Rydberg probability is a result of overlapping multiple autoionizing resonances. Their contributions depend on the 422 nm laser power and the quantum number n, which could affect the extrapolation to zero laser power as well as to large n_{eff}.

Careful inspection of the autoionization spectra reveals that the minima in the survival spectra for the nP and nF states are detuned from the core-ion resonance. The presence of the Rydberg electron within the core ion is expected to shift the $5s \rightarrow 5p$ transition by an amount that scales linearly with n_{eff}^{-3}, i.e., with the Rydberg electron-core overlap, as indicated in Table I. The measured detunings, shown in Fig. 6, are therefore plotted as a function of n_{eff}^{-3}. The measured spectra include contributions from many resonances. Therefore, small fluctuations from the linear scaling might be expected given that the contributions of each resonance to the final spectrum are slightly different depending on n_{eff}. For a given value
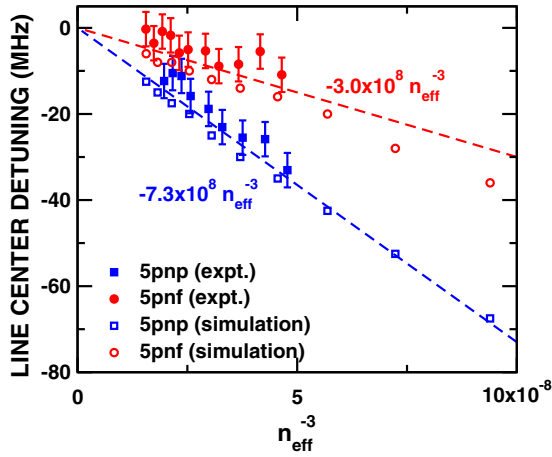
FIG. 6. Measured (filled symbols) and calculated (open symbols) detuning of the $5s\,^2S_{1/2} \rightarrow 5p\,^2P_{3/2}$ core-ion transition as a function of $1/n_{\mathrm{eff}}^3$. The dashed lines show linear fits to the data.

of n_{eff}, the detunings are larger for $5snp\,^1P$ states than for $5snf\,^1F$ states, consistent with their greater overlap with the core ion. In the limit $n_{\mathrm{eff}} \rightarrow \infty$, linear fits to the measured values yield small offsets of $\sim +5$ and $+3$ MHz from zero. Since the error bars in Fig. 6 only show the random errors and do not include the systematic error inherent in referencing the 422 nm laser to the $5s$-$5p$ transition in ^{85}Rb (estimated to be $\sim \pm 5$ MHz), the $n \rightarrow \infty$ limit appears to be consistent with the vanishing shift expected in the limit of isolated core excitation. Figure 6 also includes calculated energy shifts. The overall trends are well reproduced whereas the predicted energy shifts are slightly larger by 2–5 MHz than those observed experimentally. This could again result from the systematic errors present in the measurements.

The effect of strongly driving the core excitation with a high laser power ($P \sim 8$ mW) and a longer pulse duration (500 ns) is illustrated in Fig. 7. Most notably, weak satellite structures associated with excitation to adjacent n levels become apparent in the power-broadened Rydberg loss spectra. Such satellite structures have been previously observed in studies at lower n and their origin discussed in detail [47].

V. WAVE-PACKET DYNAMICS IN ELECTRIC FIELDS

The present apparatus allows the generation and monitoring of autoionizing Rydberg wave packets. Since the doubly excited Rydberg states are generated by (near) resonant driving of the 422 nm ion-core transition, the resulting nonstationary doubly excited state depends on the duration, T_{CP}, of the 422 nm core-exciting laser pulse (CP). This dependence is illustrated in Fig. 8 for the $5s320p\,^1P_1$ initial state. The dependence of the number of surviving Rydberg atoms observed on resonance as a function of T_{CP} is shown for several selected laser powers. Since the faster Rydberg atoms begin to move out of the 422 nm beam after ~ 0.5 μs, data were only recorded for exposure times $\lesssim 0.6$ μs. (The effect of atomic motion is not included in the master equation.) For low laser powers, the number of surviving Rydberg atoms decays approximately exponentially with increasing laser pulse width. The decay
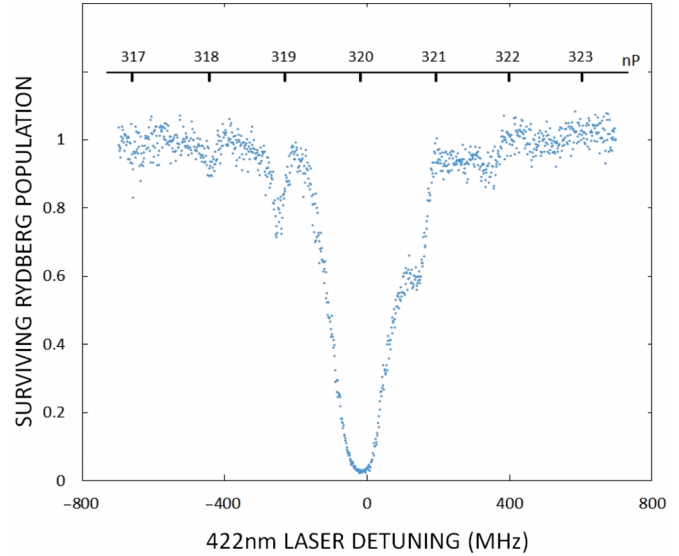

FIG. 7. Rydberg atom loss spectrum for the $5s320p\,^1P_1$ state obtained using a high 422 nm (core-exciting) laser power (~ 8 mW) and a 500-ns-long excitation pulse. For reference, the upper scale indicates the positions of neighboring nP states.

rate can be estimated by summing the autoionization rates weighted by the population of all contributing autoionizing states $\sum_a \Gamma_a \langle A_a | \rho | A_a \rangle$. For small laser powers, the population $\langle A_a | \rho | A_a \rangle$ is approximately stationary, yielding a well-defined (i.e., nearly constant) decay rate. For longer pulse widths or higher laser intensities, $\langle A_a | \rho | A_a \rangle$ decreases slowly and, correspondingly, the decay rate is expected to decrease. However, the measured results are still consistent with simple exponential decay, suggesting that any changes in the decay rate are small. The data show that at the higher 422 nm laser powers, essentially all the Rydberg atoms that are initially present undergo autoionization. (Similar behavior is observed for the neighboring $5s317f\,^1F_3$ state.)
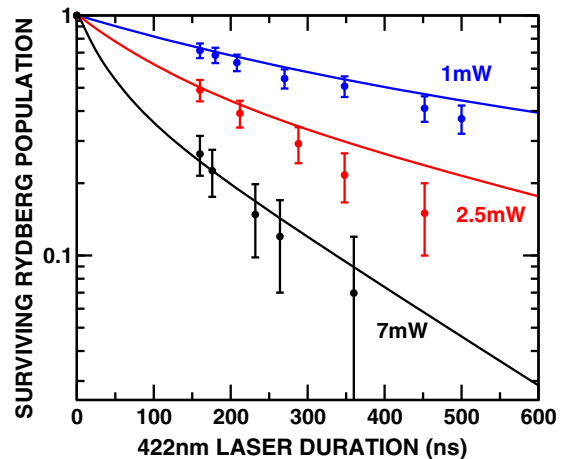

FIG. 8. Number of surviving Rydberg atoms as a function of the duration of the 422 nm core-exciting laser pulse for the (average) laser powers indicated. The symbols and the lines are the measured data and the simulated results, respectively. The initial state is $5s320p\,^1P_1$.
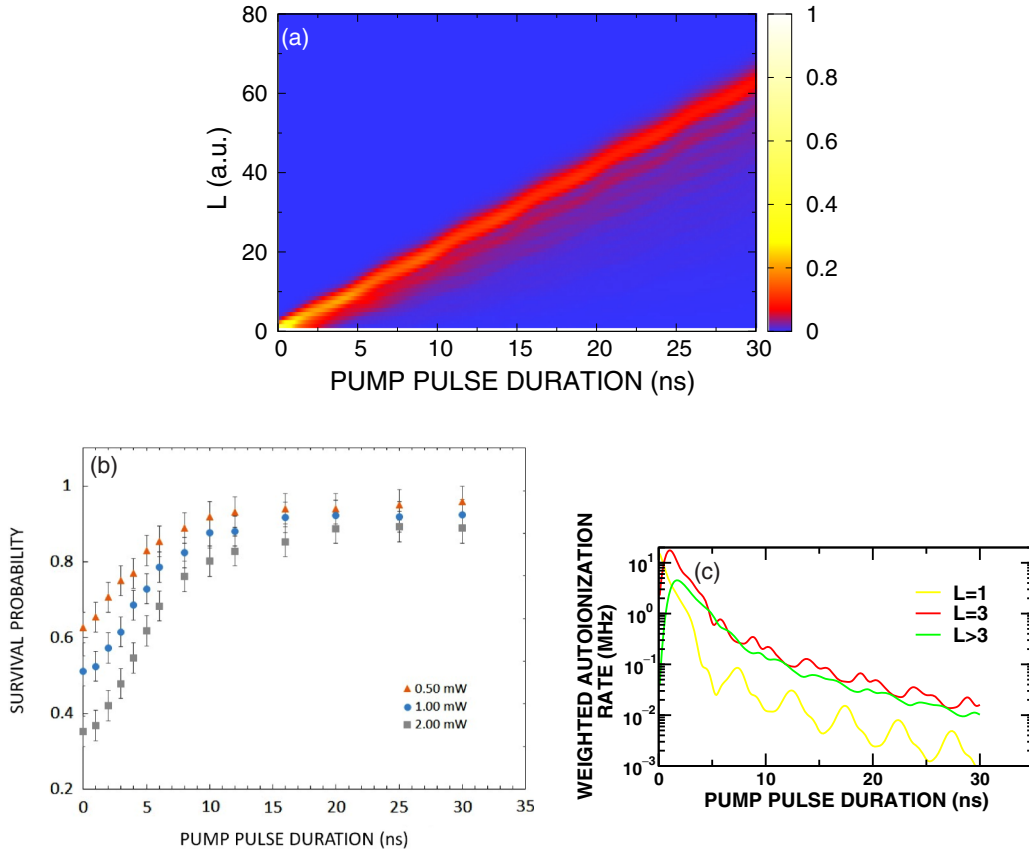
FIG. 9. (a) Calculated L distribution as a function of pump-pulse duration T_p when the initial $5s320p\,^1P_1(M_J = 1)$ state is subject to a pump pulse with a field strength of $1.8\,\mathrm{mV\,cm^{-1}}$ (see text). (b) Measured fraction of $5s320p\,^1P_1$ Rydberg atoms that survives as a function of the duration of the pump pulse (see text) for the 422 nm core-excitation laser powers indicated. The 422 nm laser pulse is 100 ns long. (c) Calculated autoionization rates for $L = 1$, $L = 3$, and $L > 3$ weighted by the L-state population in (a) as a function of pump-pulse duration T_p.

Whereas time-dependent doubly excited Rydberg wave packets can be produced by varying the duration of the core-excitation pulse after preparing a given singly excited Rydberg state (for example, the $5s320p\,^1P_1$ state), they can also be generated through the creation of a singly excited Rydberg wave packet prior to driving the core excitation which, as will be shown, allows the study of ℓ dependences in autoionization. Starting with the $5snp\,^1P_1$ initial state, a Stark wave packet can be produced by applying a weak pump field, F_p, with a rise time $T_{\mathrm{rise}} \ll T_n$, where $T_n = 2\pi n^3$ is the Kepler period, along the z (quantization) axis [48]. This pump field transforms the initial quasistationary (singly excited) Rydberg state into a wave packet that undergoes Stark precession, resulting in strong periodic variations in the magnitude of the angular momentum, i.e., L, at the Stark frequency $3nF_p$, which corresponds to the energy splitting between adjacent Stark states. This evolution can be stopped by suddenly turning off the pump pulse after some time, T_p, which freezes the L distribution. Thus, by varying the strength and/or duration of the pump pulse, it is possible to control the L distribution and the coherent superposition of L states at the instant when a doubly excited Rydberg wave packet is created by applying a core-excitation pulse. The calculated time evolution of the L distribution for an initial

$5s320p\,^1P_1(M_J = 1)$ state during a $1.8\,\mathrm{mV\,cm^{-1}}$ pump pulse is plotted in Fig. 9(a). The onset of Stark precession and the accompanying increase of the average value of L is clearly seen. We note that in the simulation, the effect of the pump pulse is modeled using a single-active-electron model [49]. Since in the singly excited Rydberg state the electron-electron interaction is much smaller than the field-induced dipole coupling, the effect of the second valence electron can be neglected. This reduction to a single-electron model allows direct simulations of Rydberg states with $n \sim 300$ without the need for any extrapolations. Figure 9(b) shows the measured Rydberg atom survival probabilities as a function of pump pulse width for several different 422 nm laser powers. The duration of the 422 nm laser pulse is 100 ns and the detuning is adjusted to yield maximum Rydberg atom destruction for each value of T_p. Since the Stark wave packet is a coherent superposition of $5snL\,^1L_L$ states and the frequency of the core-ion transition depends on L, especially for low-L states (Fig. 6), only a fraction of the Stark wave packet undergoes core excitation, i.e., those L states that are excited to autoionizing states being selected by the 422 nm laser detuning. However, since high-L states are nearly degenerate and have very small overlap with the core ion, once high-L states are dominantly populated, the whole Stark wave packet can undergo core excitation. In

practice, for short pump pulse durations T_p, the 422 nm laser is tuned to match the resonant energy shift associated with the $5snp\,^1P_1$ state (see Fig. 6). As the pump-pulse duration increases and higher-L states are populated, the laser is tuned towards the wavelength for isolated core excitation. Since the $5snd\,^1D_2$ states feature larger detunings than the $5snp\,^1P_1$ state [33], they are unlikely to be excited in this process. For near-degenerate high-L states, the autoionization rates are expected to rapidly decrease with an L^{-5} scaling. We therefore extrapolate the rate for the $5snf\,^1F_3$ state to larger L using this scaling. We note, however, that the onset of the L^{-5} behavior may lie at angular momentum larger than the $L = 3\,(F)$ state. Employing this extrapolation, the effective autoionization rate for the wave packet can be calculated for any value of T_p by summing over the rates for the different L states, weighted by their instantaneous populations [Fig. 9(c)]. Initially, the P states provide the dominant contributions to autoionization. With increasing pump-pulse duration, and hence increasing L, the F states become dominant. Further increases in pump-pulse duration lead to a population of even higher-L states, i.e., to an increase in the average value of L. However, the autoionization rates for the higher-L states are suppressed by L^{-5} and their contributions become comparable to or smaller than those from the autoionization of the $5snf\,^1F_3$ state for which the occupation probability rapidly decays. The high-L autoionization rates are mostly smaller than the radiative decay rate, $\Gamma/(2\pi) \simeq 22$ MHz, and, therefore, only a fraction of the doubly excited states will be lost through autoionization. With decreasing autoionization rate, radiative decay becomes dominant and little Rydberg atom loss is expected. This behavior is seen in the measured data [Fig. 9(b)]. Application of the pump pulse initially results in a marked decrease in the number of Rydberg atoms lost to autoionization. This number shrinks rapidly as the duration of the pump pulse is increased. For a pump-pulse duration $T_p \gtrsim 15$ ns, the fraction of surviving Rydberg atoms reaches a near plateau and thereafter increases only slowly with further increases in pump-pulse width. For example, pump-pulse durations of ~ 80 ns are required to obtain survival fractions of ~ 0.95-0.99 for the present range of laser powers. Thus, whereas application of a pump pulse dramatically decreases the fraction of Rydberg atoms lost to autoionization, autoionization is not completely suppressed. This results because decay from the core-ion $5p\,^2P_{1/2}$ level can lead to population of the $4d\,^2D_{3/2}$ state, which can also be followed by autoionization (Fig. 1). Indeed, an estimate using the master equation extended to include the $4d_{3/2}n\ell_j$ autoionizing states indicates a 2.6% to 5.8% occupation probability for $4d_{3/2}n\ell_j$ states, depending on laser power. Since the $4d\,^2D_{3/2}$ state is long lived, it can continue to induce autoionization even after termination of the 422 nm laser pulse. Thus, given the relatively long-time delay ($\sim 10\,\mu$s) between application of the 422 nm laser pulse and start of the field ionization ramp, even small autoionization rates can lead to measurable loss. Nonetheless, the data do clearly demonstrate that autoionization rates decrease rapidly with increasing L.

The L dependence of the autoionization rate for doubly excited Rydberg states can also be explored in a time-independent setting by utilizing the adiabatic limit of Stark switching

and creating $5snf\,^1F_3$ states in a weak applied dc electric field. As the field is increased, the $5snf\,^1F_3$ states evolve into extreme redshifted quasihydrogenic Stark states that are strongly polarized, i.e., have a large dipole moment, and that display a near-linear Stark energy shift. The resulting effect on the excitation spectrum and on the autoionization loss spectrum is illustrated in Fig. 10 for several values of applied field. Each loss spectrum was recorded following identical 100-ns-long core-excitation pulses. In the absence of a dc field, the Rydberg excitation spectrum contains sharp peaks corresponding to excitation of $5snf\,^1F_3$ and $5snp\,^1P_1$ states. As the applied field increases, the field-dressed $5snf\,^1F_3$ initial state, which will (for simplicity) still be labeled by its zero-field angular momentum "$5snf\,^1F_3$" designation, merges with the neighboring Stark manifold and acquires increasingly high-L character. In consequence, its photoexcitation rate is decreased, resulting in a decrease in the size of its associated peak in the excitation spectrum. At the same time, a broad feature appears in the spectrum that results from excitation of the manifold of Stark states. In addition, a small peak associated with excitation of "$5s(n + 2)d\,^1D_2$" states appears. In the presence of a dc field, the autoionizing states are coupled by dipole transitions and form a mixed set of eigenstates. With increasing electric field strength, the dipole coupling becomes dominant compared to both the spin-orbit coupling of the Rydberg electron and the electron-electron interaction. In this limit, the orbital motion of the Rydberg electron is nearly independent of its spin and the inner electron. The same applies to the initial singly excited Rydberg "$5snf\,^1F_3$" state. Therefore, the core-excitation probability becomes independent of the outer electron state. Consequently, though the decrease in the surviving Rydberg population results from a convolution of the core-excitation and the autoionization probabilities, it can be used as a direct measure of the autoionization rate. However, in such a limit, the oscillator strengths for excitation of the initial "$5snf\,^1F_3$" states become extremely small. Therefore, to produce significant numbers of Rydberg atoms, very weak fields $F_{\text{dc}} \simeq 100$ and 140 μV/cm are used. These are considerably smaller than the field strength $F_{\text{cross}} = 1/(3n^5)$ at which states in neighboring manifolds first cross. For $n = 310$, $F_{\text{cross}} \simeq 600\,\mu$V/cm. The dipole coupling strength induced by the dc fields is about $(3/2)n_{\text{eff}}^2 F_{\text{dc}} \sim 18$–25 MHz, which is comparable to or smaller than the electron-electron interaction and the spin-orbit coupling, $\delta/n_{\text{eff}}^3 \sim 30$ MHz (Table I). This leads to energy shifts for autoionizing states accessible from the "$5snf\,^1F_3$" state that are similar to those for the zero dc field case. With increasing F_{dc}, a dramatic decrease in the number of atoms that undergo autoionization is observed (Fig. 10). This results from the increasing high-L character of the "$5snf\,^1F_3$" states, which suppresses the autoionization rate [24]. Indeed, the calculations show that the "$5snf\,^1F_3$" state at $F_{\text{dc}} = 100\,\mu$V/cm has fractional populations of about 54% in the F state and 34% in the G state, whereas at $F_{\text{dc}} = 140\,\mu$V/cm, these become 38% in the G state, 35% in the F state, and 17% in the H state. The measured data confirm that the autoionization rates are comparable to the radiative decay rate below $F_{\text{dc}} = 100\,\mu$V/cm. At higher fields, radiative decay dominates and little sign of autoionization is seen. Indeed, when the autoionization rate for strongly L-mixed Stark states
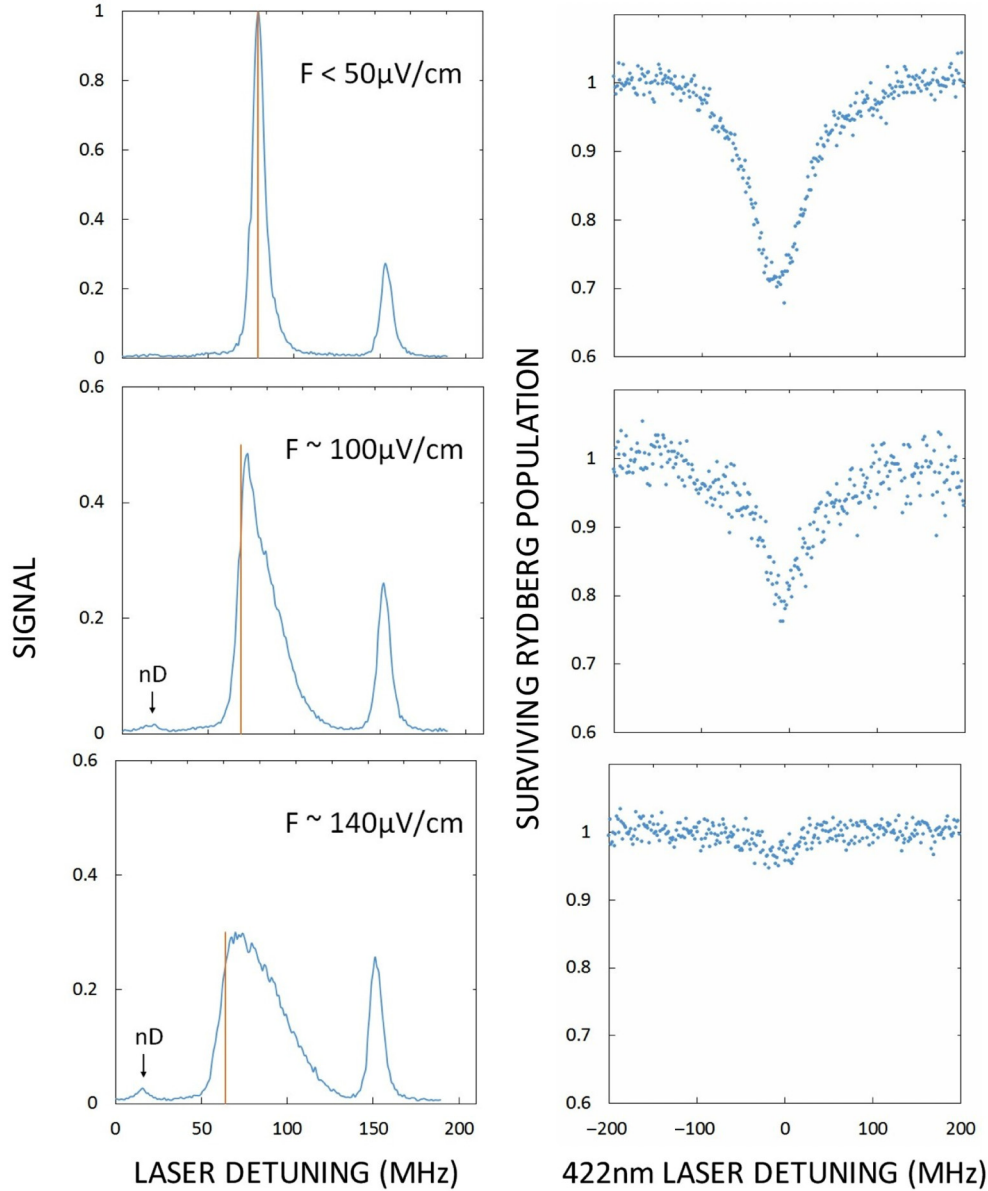
FIG. 10. Left column: Excitation spectra for "$5s310f\ {}^1F_3$" initial states recorded using identical laser powers in the presence of the dc fields indicated (note the change in scale of the vertical axis). The positions of the vertical lines represent the energy of the field-dressed "$5s310f\ {}^1F_3$" state and its height represents the overlap between the field-dressed and the field-free $5s310f\ {}^1F_3$ states. Right column: Rydberg atom autoionization loss spectra recorded with the Rydberg excitation lasers tuned to the points indicated by the lines in the corresponding excitation spectra.

is approximated by an L-averaged autoionization rate [31], the rate is only $\sim 0.3\%$ of that for the field-free $5snf\ {}^1F_3$ state [$\Gamma/(2\pi) \sim 60$ MHz] and is negligible compared to the radiative decay rate of the isolated core ion, $\gamma/(2\pi) \sim 22$ MHz. The present observation that the autoionization of high-L Rydberg states is suppressed complements the earlier observation that the presence of stray electric fields can strongly enhance dielectronic recombination (DR). The admixture of high-L states introduced by stray fields suppresses autoionization, thereby favoring radiative stabilization of the resonant intermediate state formed though electron-ion collisions. The very same mechanism is operational here in very-high-n autoionizing Rydberg wave packets.

VI. CONCLUSIONS AND OUTLOOK

Autoionization of very-high-n doubly excited Rydberg states is studied. For high-n Rydberg states, the radiative decay rate becomes comparable to the autoionization rate. In this limit, the surviving Rydberg population provides a measure of autoionization. Since several autoionizing resonances overlap with each other due to line broadening induced by radiative decay, the excitation dynamics has to be studied carefully to accurately interpret the width and the position of the measured spectra. The dramatic decrease in autoionization rates observed with increasing L suggests that by initially placing one electron in a near circular very-high-n, high-L orbit, it should be possible to excite the remaining valence electron to produce a long-lived doubly excited state. Excitation of the inner electron to

degenerate high-ℓ states produces an inner electron wave function that is readily polarizable. The polarized inner electron can then interact with the high-L Rydberg electron, thereby suppressing the dispersion of the outer electron wave function forming a planetary atom. The results of the present study suggest that the formation of such long-lived planetary atoms that are stable against autoionization may come within reach.

[1] F. B. Dunning, C. O. Reinhold, S. Yoshida, and J. Burgdörfer, Am. J. Phys. **78**, 796 (2010).

[2] M. Kalinski, J. H. Eberly, J. A. West, and C. R. Stroud, Jr., Phys. Rev. A **67**, 032503 (2003).

[3] J. J. Mestayer, B. Wyker, J. C. Lancaster, F. B. Dunning, C. O. Reinhold, S. Yoshida, and J. Burgdörfer, Phys. Rev. Lett. **100**, 243004 (2008).

[4] B. Wyker, S. Ye, F. B. Dunning, S. Yoshida, C. O. Reinhold, and J. Burgdörfer, Phys. Rev. Lett. **108**, 043001 (2012).

[5] J. A. West, Z. D. Gaeta, and C. R. Stroud, Jr., Phys. Rev. A **58**, 186 (1998).

[6] I. C. Percival, Proc. R. Soc. London A **353**, 289 (1977).

[7] U. Eichmann, P. Brockmann, V. Lange, and W. Sandner, J. Phys. B **22**, L361 (1989).

[8] K. Richter and D. Wintgen, Phys. Rev. Lett. **65**, 1965 (1990).

[9] U. Eichmann, V. Lange, and W. Sandner, Phys. Rev. Lett. **68**, 21 (1992).

[10] M. Seng, M. Halka, K.-D. Heber, and W. Sandner, Phys. Rev. Lett. **74**, 3344 (1995).

[11] G. Tanner, K. Richter, and J.-M. Rost, Rev. Mod. Phys. **72**, 497 (2000).

[12] D. Janby, L. B. Madsen, and V. N. Ostrovsky, Phys. Rev. A **73**, 062708 (2006).

[13] K. Zimmermann, P. Lugan, F. Jörder, N. Heitz, M. Schmidt, C. Bouri, A. Rodriguez, and A. Buchleitner, J. Phys. B **48**, 025001 (2015).

[14] A. Bolovinos, A. Jimoyiannis, S. Assimopoulos, and P. Tsekeris, J. Phys. B **25**, L533 (1992).

[15] R. van Leeuwen, W. Ubachs, and W. Hogervorst, J. Phys. B **27**, 3891 (1994).

[16] M. Aymar, C. H. Greene, and E. Luc-Koenig, Rev. Mod. Phys. **68**, 1015 (1996).

[17] S. Cohen, M. Aymar, A. Bolovinos, M. Kompitsas, E. Luc-Koenig, H. Mereu, and P. Tsekeris, Eur. Phys. J. D **13**, 165 (2001).

[18] S. N. Pisharody and R. R. Jones, Science **303**, 813 (2004).

[19] J. Murray-Krezan, J. Kelly, M. R. Kutteruf, and R. R. Jones, Phys. Rev. A **75**, 013401 (2007).

[20] J. Millen, G. Lochead, and M. P. A. Jones, Phys. Rev. Lett. **105**, 213004 (2010).

[21] G. Lochead, D. Boddy, D. P. Sadler, C. S. Adams, and M. P. A. Jones, Phys. Rev. A **87**, 053409 (2013).

[22] T. F. Gallagher, *Rydberg Atoms* (Cambridge University Press, New York, 1992).

[23] R. R. Freeman and D. Kleppner, Phys. Rev. A **14**, 1614 (1976).

[24] W. E. Cooke and T. F. Gallagher, Phys. Rev. A **19**, 2151 (1979).

[25] M. Poirier, Phys. Rev. A **38**, 3484 (1988).

[26] R. R. Jones and T. F. Gallagher, Phys. Rev. A **38**, 2846 (1988).

[27] I. Bialynicki-Birula and Z. Bialynicka-Birula, Phys. Rev. A **81**, 012121 (2010).

[28] J. Dubau and S. Volonte, Rep. Prog. Phys. **43**, 199 (1980).

[29] D. S. Belic, G. H. Dunn, T. J. Morgan, D. W. Mueller, and C. Timmer, Phys. Rev. Lett. **50**, 339 (1983).

[30] J. G. Story, B. J. Lyons, and T. F. Gallagher, Phys. Rev. A **51**, 2156 (1995).

[31] K. LaGattuta, I. Nasser, and Y. Hahn, J. Phys. B **20**, 1565 (1987).

[32] E. Y. Xu, Y. Zhu, O. C. Mullins, and T. F. Gallagher, Phys. Rev. A **33**, 2401 (1986).

[33] E. Y. Xu, Y. Zhu, O. C. Mullins, and T. F. Gallagher, Phys. Rev. A **35**, 1138 (1987).

[34] K. J. Reed, M. H. Chen, and D. L. Moores, Phys. Rev. A **41**, 550 (1990).

[35] P. M. Dehmer, W. L. Luken, and W. A. Chupka, J. Chem. Phys. **67**, 195 (1977).

[36] G. Lindblad, Comm. Math. Phys. **48**, 119 (1976).

[37] B. Simon, Phys. Lett. A **71**, 211 (1979).

[38] S. Ye, X. Zhang, F. B. Dunning, S. Yoshida, M. Hiller, and J. Burgdörfer, Phys. Rev. A **90**, 013401 (2014).

[39] A. Sinclair, M. Wilson, and P. Gill, Opt. Commun. **190**, 193 (2001).

[40] A. Gallagher, Phys. Rev. **157**, 24 (1967).

[41] J. E. Sansonetti, J. Phys. Chem. Ref. Data **41**, 013102 (2012).

[42] E. Condon and G. Shortley, *The Theory of Atomic Spectra* (Cambridge University Press, New York, 1951).

[43] J. S. Cohen, Phys. Rev. A **64**, 043412 (2001).

[44] P. G. Burke, A. Hibbert, and W. D. Robb, J. Phys. B **4**, 153 (1971).

[45] K. Bartschat, M. R. H. Rudge, and P. Scott, J. Phys. B **19**, 2469 (1986).

[46] R. Jastrow, Phys. Rev. **73**, 60 (1948).

[47] N. H. Tran, P. Pillet, R. Kachru, and T. F. Gallagher, Phys. Rev. A **29**, 2640 (1984).

[48] B. Wyker, S. Ye, T. J. McKinney, F. B. Dunning, S. Yoshida, C. O. Reinhold, and J. Burgdörfer, J. Phys. B **44**, 184002 (2011).

[49] M. Hiller, S. Yoshida, J. Burgdörfer, S. Ye, X. Zhang, and F. B. Dunning, Phys. Rev. A **89**, 023426 (2014).